Journal of Alloys and Compounds 480 (2009) 306–310

Contents lists available at ScienceDirect

Journal of Alloys and Compounds

journal homepage: www.elsevier.com/locate/jallcom

The microstructure development in $Fe_{32}Cu_{20}Ni_{28}P_{10}Si_5B_5$ immiscible alloy and possibilities of formation of amorphous/crystalline composite

Krzysztof Ziewiec[a,*], Zbigniew Kędzierski[b]

[a] Institute of Technology, Pedagogical University of Cracow, ul. Podchorążych 2, 30-084 Krakow, Poland
[b] AGH University of Science and Technology, Faculty of Metal Engineering and Industrial Computer Science, 30 Mickiewicza Avenue, 30-059 Krakow, Poland

ARTICLE INFO

Article history:
Received 28 November 2008
Received in revised form 15 January 2009
Accepted 23 January 2009
Available online 12 February 2009

Keywords:
Melt spinning
Transmission electron microscopy (TEM)
X-ray diffraction (XRD)
Nanocomposite
Mechanical properties

ABSTRACT

The microstructures of $Fe_{32}Cu_{20}Ni_{28}P_{10}Si_5B_5$ alloy representing the effects of slow cooling after arc melting and rapid cooling after melt spinning are shown. The slow cooling rate resulted in the fractal-like structures formed by the Fe-rich regions and Cu-rich regions typical for the alloying systems with a miscibility gap. The structures observed after rapid cooling were dependent on ejection temperatures of the alloy just before the melt spinning process. The lower ejection temperatures created crystalline structures separated into Fe-rich and Cu-rich regions as a result of rapid cooling within the miscibility gap. The higher ejection temperatures contributed to formation of amorphous/crystalline composite. The crystalline spherical precipitates were found to be predominantly Cu-base solid solution.

1. Introduction

Metallic alloys with the amorphous structure present excellent properties in comparison with their traditional crystalline counterparts. They are very attractive as regards high strength, high elastic limit and soft magnetism [1–3]. However, for some applications, it would be useful to produce a composite material, joining the properties of the amorphous matrix and a highly dispersed fine crystalline phase. This could be potentially useful in such cases as improving ductility by introducing a soft crystalline phase or increasing coercivity in hard magnet structures with use of a paramagnetic phase. Such works have already been made in order to improve the ductility by means of ductile crystalline phase formed in situ [4,5]. The composites can be formed alternatively, by introducing the particles ex situ prior to casting [4–6], or by formation of the crystalline phase in situ. The latter, in turn, can be carried out by crystallization of the amorphous matrix or the formation of the crystalline phase during casting [7–11]. The formation of primary dendritic crystals may not be effective as their formation sometimes is suppressed due to the existence of the eutectic zone. Anther idea to form a composite is using an immiscible alloy system. Production of the composite directly from the liquid state, using miscibility gap is justified as regards energy saving because no additional heat treatment to produce the fine crystalline phase is necessary. So far, there are reports on formation of two-phased glassy composites in Ni–Nb–Y system [12,13], Y–Ti–Al–Co system [14] and iron-based Fe–Cu–Ni–Si–Sn–B–Y amorphous/crystalline composite [15]. As regards the iron-based alloys, it can be found [15] that glass formation is possible in iron-metalloid ternary Fe–Si–P, Fe–Si–B, Fe–P–B, Fe–Ni–P, Fe–Ni–B systems. On the other hand, Fe–Cu–P, Fe–Cu–Si, Fe–Cu–B systems have a miscibility gap in the liquid phase [16], therefore we considered the Fe–Cu–Ni–P–Si–B system for experiment. In order to forecast the behavior of the multi-component system it is useful to know the enthalpies of mixing in liquid binary systems (see Table 1).

The Fe–Cu–Ni–P–Si–B system will probably show a tendency for separation into Fe-rich and Cu-rich regions due to a positive enthalpy of mixing between iron and copper as it is observed in ternary Fe–Cu–P, Fe–Cu–Si [16]. On the other hand, relatively high negative enthalpy of mixing for iron and nickel with P, Si and B as well as nickel and copper with phosphorus may facilitate the amorphization of the alloy. Therefore, the aim of the work is to study the effects of the mixing the above mentioned elements in the $Fe_{32}Cu_{20}Ni_{28}P_{10}Si_5B_5$ alloy in order to make the amorphous/crystalline composite.

2. Experimental

The $Fe_{32}Ni_{28}Cu_{20}P_{10}Si_5B_5$ alloy was prepared by arc melting of pure elements 99.95 wt.% Ni, 99.95 wt.% Cu, 99.95 wt.% Fe, 99,999 wt.% Si and Fe–P, Fe–B, Ni–P, Ni–B master alloys. The alloy was melted five times under titanium gettered argon atmosphere. Morphology and chemical composition of the cross-section of the ingot were analysed with scanning electron microscope (SEM) Philips XL 30 with

* Corresponding author. Tel.: +48 12 662 61 14.
E-mail address: kziewiec@gmail.com (K. Ziewiec).

0925-8388/$ – see front matter © 2009 Elsevier B.V. All rights reserved.
doi:10.1016/j.jallcom.2009.01.139

Table 1
Calculated enthalpies of mixing for equiatomic liquids in binary systems, kJ/mol [17,18[a]].

	Fe	Cu	Ni	P	Si	B
Fe	–	+13.0	−2.0	−31.0	−18.0	−11.0
Cu		–	+4.0	−17.5	−10.0	+16.0[a]
Ni			–	−26.0	−23.0	−9.0

[a] Mixing enthalpy for Cu–B is approximated based on [18].

X-ray microanalyser Link ISIS-EDX. The alloy was melt-spun in helium atmosphere with the linear velocity of 33 m/s, ejection pressure 150 kPa, crucible and hole diameter 0.7 mm starting from different temperatures i.e.: 1273 K, 1323 K, 1360 K, 1403 K, 1513 K, 1563 K, 1647, 1731 K, where the pouring temperature was controlled with use of RAYTECH MARATHON series BH2MR1SBSF two-colour pyrometer. The microstructure of the arc melt ingot and melt melt-spun ribbons were again investigated by means of scanning electron microscope. The melt-spun alloy was investigated by means of the JEOL 300 kV transmission electron microscope (TEM). X-ray diffraction was performed on the DRON-3 diffractometer using Cu Kα radiation filtered by the bent single crystal LiF linearly focusing monochromator on the detector side. The scattering angle 2Θ was varied between 35° and 55° with the constant step of 0.05°. Scans were performed in the Θ–2Θ mode. The melt-spun ribbons were then investigated by means of differential thermal analysis (DTA-STD 2960 TA Instruments) at the heating rate 20 K/min.

3. Results

The primary microstructure of the $Fe_{32}Ni_{28}Cu_{20}P_{10}B_5Si_5$ alloy droplet is presented in Fig. 1. The surface fractal [19] morphology of the alloy consists of the bright globular regions marked "A" included in the darker matrix marked "B". EDS Mapping of elements indicates that, the globular "A" regions were Cu-rich liquid impoverished in iron. It is also observed, that the globular "A" regions contain significantly smaller quantity of phosphorus and nickel than "B" regions. It seems, however, that content of silicon in "A" regions is only slightly lower than in iron-base matrix "B". As regards boron, it is not detected by the analysis, however, it can be expected that due to negative mixing enthalpy for Fe–B (−11 kJ/mol) and positive one for Cu–B (+16 kJ/mol) (Table 1) boron will be strongly attracted in iron-rich "B" regions. Therefore, before solidification, the Fe-rich liquid matrix, regions "B", were also enriched in nickel, phosphorus and probably boron. The silicon content seems to be a little higher in Fe-rich regions, although due to a small difference in mixing enthalpies and small silicon content in the alloy (5 at.%), the distribution between "A" and "B" regions was similar (Fig. 1f).

The light microphotographs of the ribbons, melt-spun starting from the different melt temperatures are shown in Fig. 2. At lower temperatures i.e.: 1273 K, 1323 K and 1360 K the appearance of the cross-sections are inhomogeneous. For the ribbons spun from 1273 K and 1323 K it is even possible to observe relatively large copper-base globular regions of few microns. For the inhomogeneous ribbons cast from 1273 K, 1323 K (Fig. 3) and 1360 K, the tendency for segregation of chemical elements is similar as in case of as-cast of the arc melt droplet, i.e. we observe copper-rich "A" regions and iron-rich matrix. Copper-rich regions are also impoverished in phosphorus and nickel. However, distribution of silicon is apparently uniform. For the higher temperatures i.e.: 1403 K, 1513 K, 1563 K, 1647 K and 1731 K a homogeneous structure of the ribbon with a fine distribution of particles was obtained and TEM observations revealed uniform distribution of very thin crystalline particles of the average size of 74 ± 4 nm within amorphous matrix. Electron diffraction patterns show a broad diffusive rings typical for the amorphous structure (Fig. 4a). Majority of the spherical particles could be identified as Cu-base (Fm-3m) (Fig. 4a). Moreover, it was possible to find a few spherical particles of M_3P (I-4) (Fig. 4b).

The X-ray diffraction patterns from the $Fe_{32}Ni_{28}Cu_{20}P_{10}Si_5B_5$ ribbons are presented in Fig. 5. For reference, the melt-spun ribbon melt-spun from 1647 K was annealed at 1073 K during 1 h in order to obtain the phase composition close to equilibrium. The diffraction pattern has got very clear and sharp peaks that allow for identification of the following phases isomorphic with: Cu-base solid solution (Fm-3m), $Fe_{50}Ni_{50}$ (Fm-3m), Ni_3P (I-4), $Fe_{95}Ni_5$ (Im-3m) and $Ni_{30.7}Si_{12.3}$ (P321). The diffraction patterns corresponding to the lowest temperatures of melt spinning i.e. 1273 K and 1323 K have poorly formed peaks due to the low volume fraction of crystalline phase included in amorphous matrix, although it is possible to attribute their position to the phases existing in the sample annealed at 1073 K. Diffraction patterns for the alloys melt-spun from higher temperature have two poorly formed peaks for the values of 2Θ close to 43–44°, 50–51°, i.e. corresponding to Cu (Fm-3m), FeNi (Fm-3m) for (1 1 1) and (2 0 0), respectively. The peak near 43° may also correspond to Ni_3P (1 1 2).

DTA results of $Fe_{32}Ni_{28}Cu_{20}P_{10}Si_5B_5$ cast from 1647 K are presented in Fig. 6. The curve shows one-step crystallization of the amorphous matrix with the onset at $T_x = 744$ K and crystallization peak at $T_p = 756$ K. Melting of the alloy occurs in a two-step sequence with the beginning at $T_m = 1156$ K and the end

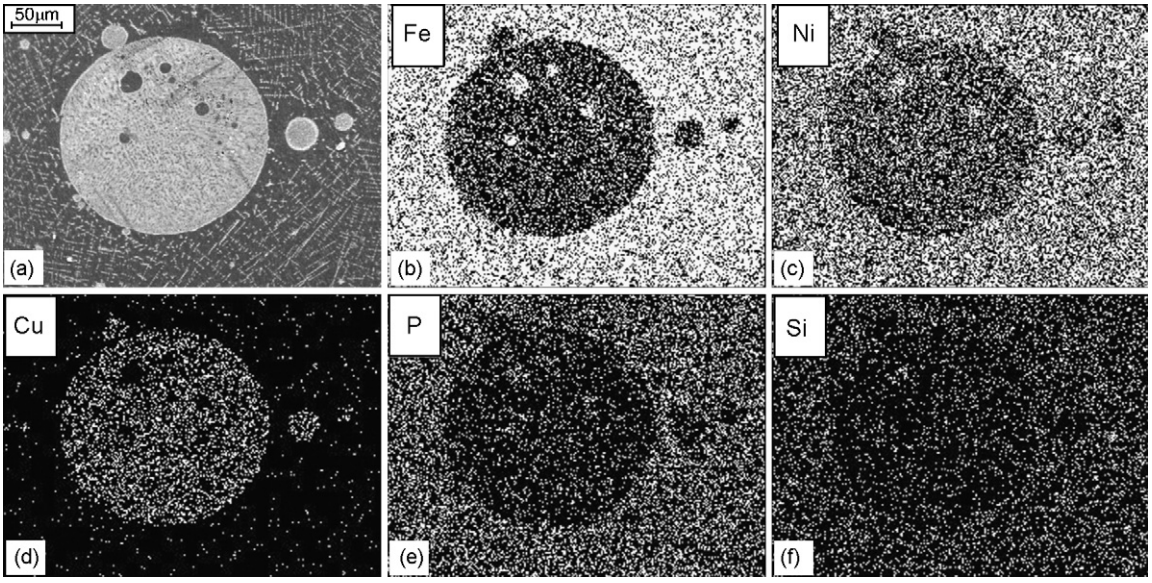

Fig. 1. (a–f) SEM microstructure with mapping of elements on the cross-section of $Fe_{32}Cu_{20}Ni_{28}P_{10}Si_5B_5$ massive arc melt droplet.

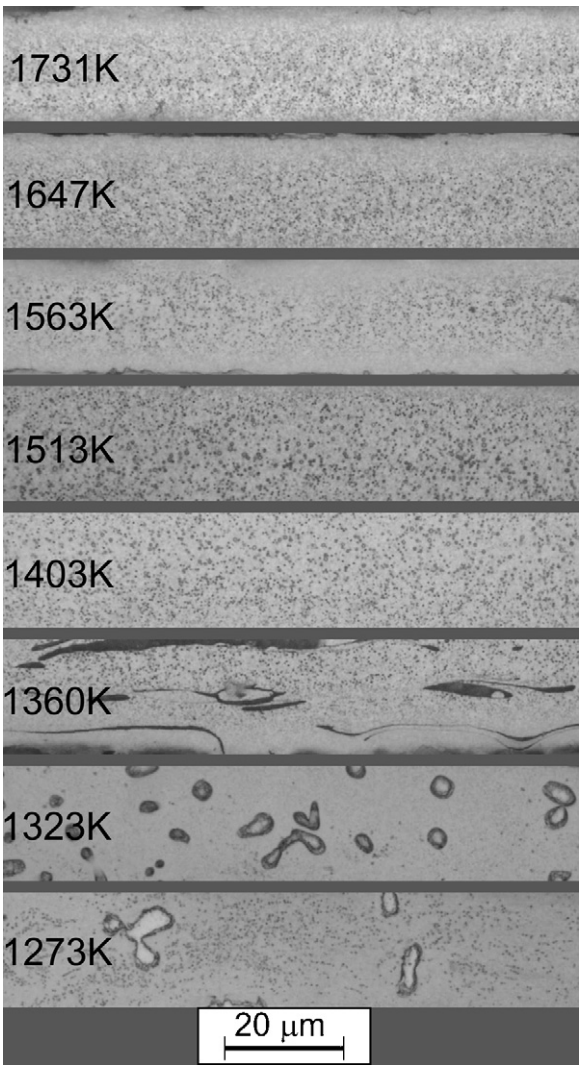

Fig. 2. Light microscope images of $Fe_{32}Cu_{20}Ni_{28}P_{10}Si_5B_5$ melt-spun ribbons after different ejection temperatures before melt spinning process.

at T_l = 1156 K. A small endothermic peak is also observed at higher temperatures with the onset at $T_{d\text{-}onset}$ = 1358 K and end-set at $T_{d\text{-}end\text{-}set}$ = 1373 K occurring probably due to dissolution of melts that were insoluble at lower temperatures. In the binary monotectic alloys the transformation from crystalline state to a uniform liquid phase may follow as a result of a multi-step reaction including as many as four stages, i.e.: melting of eutectics (peritectics), dissolution in the liquid of off-eutectic crystals, monotectic reaction, and mutual dissolution of insoluble liquids.

4. Discussion

Microstructure of the massive droplet, contained regions that separated in a liquid state into two insoluble liquids – Cu-rich and Fe-rich. Generally, Fe-rich regions attracted more strongly all the alloying elements except for copper. This is in agreement with the expectations based on the enthalpies of mixing, which are substantially more negative for Fe–X and Ni–X pairs than Cu–X pairs (where X = B, P, Si). This is probably the reason for favored formation of Fe–X regions with some amount of nickel. The positive values of mixing enthalpies are reported for equiatomic compositions of Fe–Cu, Cu–B and Ni–Cu i.e.: $\Delta H^{mix}_{\{Fe-Cu\}} = +13$; $\Delta H^{mix}_{\{Cu-B\}} = +16$ and $\Delta H^{mix}_{\{Cu-Ni\}} = +4$, respectively. This can explain the repelling copper from Fe-rich regions and the repelling iron from Cu-rich regions. It is also possible that almost entire content of boron is located in Fe-rich regions.

Formation of surface fractal structure is observed, which is typical for the systems with a miscibility gap [19]. As the cooling rate after the arc melting is relatively slow (order of 100 K/s), even the alloy with the initial temperature assuring a single homogeneous liquid will separate, at first into two liquids, and then that melts will separate into the range of compositions depending on the slope of the miscibility gap curve. This can finally develop the fractal-like structure with a quite substantial scatter of sizes (e.g.: from a few mm to a few μm) and indeed, we found this in our arc melt sample. However, in case of $Fe_{32}Ni_{28}Cu_{20}P_{10}Si_5B_5$ melt-spun ribbons, we observed development of structures. For the melt spinning at lower temperatures, separation in the liquid state produced Fe-rich regions and Cu-rich regions and the spatial distribution was inhomogeneous, similarly as in arc melt sample. The melt spinning technique caused mainly grain refinement of Cu-rich regions (Figs. 2 and 3), which is also reflected in poor formation of the

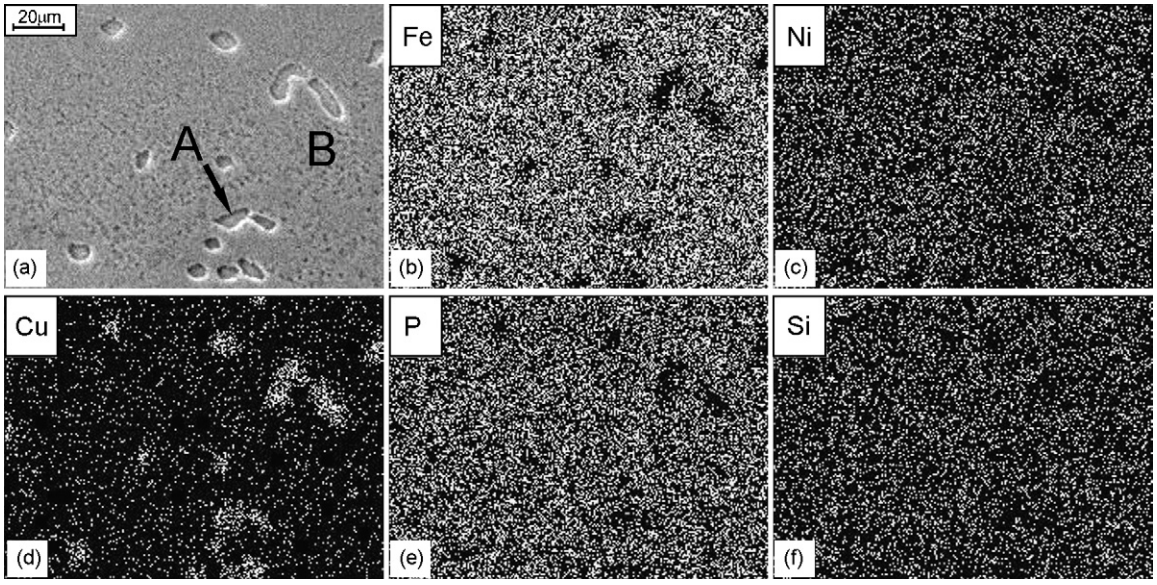

Fig. 3. (a–f) SEM microstructure with mapping of elements on the cross-section of the $Fe_{32}Cu_{20}Ni_{28}P_{10}Si_5B_5$ melt-spun ribbon ejected at 1323 K.

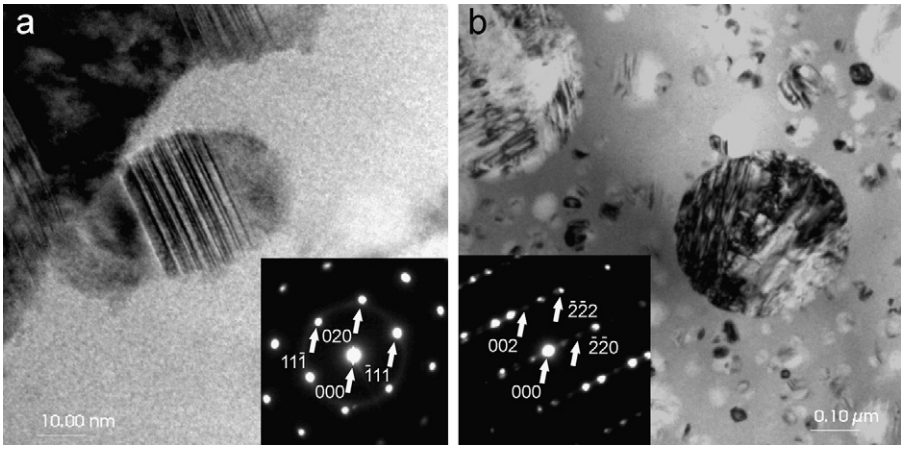

Fig. 4. TEM micrographs of the $Fe_{32}Cu_{20}Ni_{28}P_{10}Si_5B_5$ melt-spun ribbon ejected at 1647 K where; (a) majority of the particles could be identified as spherical shape Cu-base (Fm-3m) solid solution; (b) and some minor particles were also spherical M_3P (I-4) phosphides.

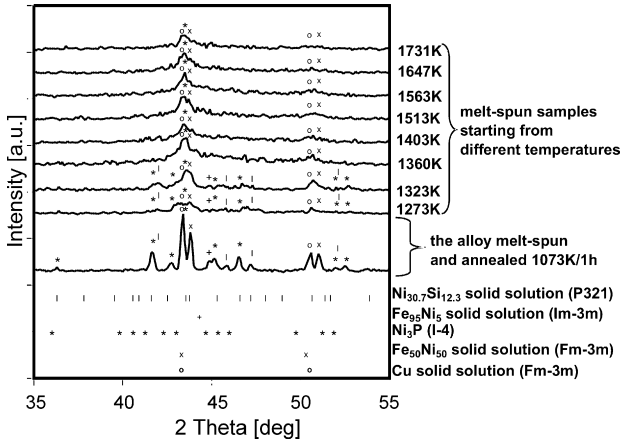

Fig. 5. X-ray patterns for melt-spun ribbons ejected at different temperatures with phase identification. The XRD of the ribbon ejected at 1647 K and annealed at 1073 K/1 h is attached for reference as well crystallized sample of the $Fe_{32}Cu_{20}Ni_{28}P_{10}Si_5B_5$ alloy.

diffraction peaks. Generally it is still possible to identify similar phases as in a fully crystallized sample. However, the increase of the melt spinning temperature to the values as high as 1403 K causes homogenization of the structure visible on light micrographs (Fig. 2). X-ray diffraction patterns for the samples melt-spun from the higher temperatures (>1403 K) do not allow phase identification, because they only have two broad peaks near the positions of Cu-base solid solution. The peaks can be close to peak positions in Fe–Ni solid solution and M_3P type phosphide. More detailed structure examination of the homogeneous ribbons under TEM confirmed the majority of the fine particles consists of Cu-base solid solution (Fig. 4a) and some of them are M_3P phosphides (Fig. 4b). The amorphous matrix was probably Fe-rich product, highly alloyed in glass forming agents like P, Si and boron. The uniform distribution found in the ribbons melt-spun from the temperatures higher than 1403 K in contrast to the non-uniform structure obtained after ejection from temperatures 1360 K and lower, can be explained by the fact that in the former case the alloy was cast from homogenous melt above the miscibility gap in the system. The similar observation was found also in Fe–Cu–Si–B–Al–Ni–Y alloys [20].

As it is found from DTA curve, the amorphous matrix crystallizes (T_x = 744 K, T_p = 756 K) and the entire alloy melts between T_m = 1156 K and T_x = 1195 K. However, as it was found from the experiment with differing ejection temperatures, there is a temperature range, where non-uniform structure after melt spinning is obtained. This corresponds, probably to the miscibility gap for the $Fe_{32}Ni_{28}Cu_{20}P_{10}Si_5B_5$ alloy. Thus, after dissolution of the liquids, one liquid provides the uniform structure of the ribbons during the melt spinning. The temperature range, where the dissolution occurs is visible on DTA as a small endothermic effect [21,22]. In the present study it was between $T_{d\text{-}onset}$ = 1358 K and

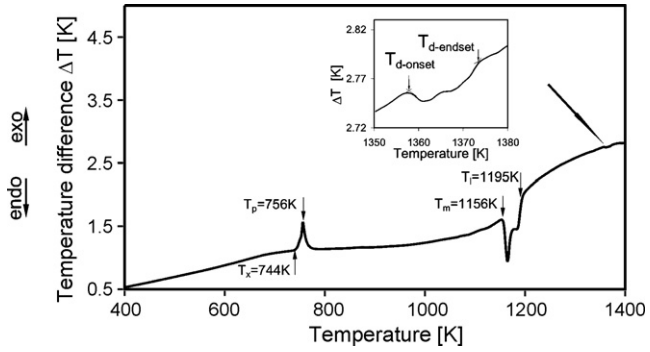

Fig. 6. DTA trace for the $Fe_{32}Cu_{20}Ni_{28}P_{10}Si_5B_5$ melt-spun ribbon ejected at 1647 K.

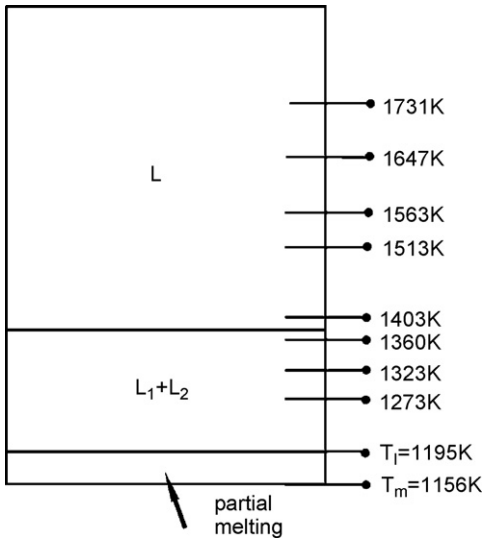

Fig. 7. Schematic presentation of the onset of partial melting, miscibility temperature range and homogeneous liquid temperature range, based on the microstructural observations of ribbons melt-spun at the different ejection temperatures.

$T_{d\text{-end-set}}$ = 1373 K (Fig. 6). The sequence of the partial melting, existence of insoluble liquids "$L_1 + L_2$", and uniform liquid as well as the temperatures of ejection before the melt spinning marked with (●) is presented in Fig. 7. With comparison to the ternary Fe–Cu–P system [16], where the miscibility region seems to be very large, the $Fe_{32}Ni_{28}Cu_{20}P_{10}Si_5B_5$ alloy was prepared by partial substitution of iron with nickel and phosphorus with silicon and boron. As a result, a substantially lower melting range $T_l - T_m$ as well as a narrower miscibility gap with comparison to the Fe–Cu–P system was obtained.

5. Conclusions

1. The primary microstructure of the $Fe_{32}Ni_{28}Cu_{20}P_{10}Si_5B_5$ alloy droplet after a relatively slow cooling (10^2 K/s) arc melting process has the fractal-like morphology formed as a result of separation of liquids occurring during relatively slow cooling.
2. The primary structure of the alloy after arc melting consists of the Fe-rich matrix and spherical Cu-rich regions. The Fe-rich regions are more alloyed by the constituents of the alloy than Cu-rich regions. Silicon has the most uniform distribution between the Fe-rich and Cu-rich colonies. Formation of such regions is in agreement with expectations based on the enthalpies of mixing between the pairs of the alloying constituents.
3. The microstructure of the alloy cooled with a high rate 10^5 K/s depends on ejection temperature before the melt spinning process. Low ejection temperatures favor formation of a non-uniform crystalline structure where Fe-rich matrix and Cu-rich regions of few μm are observed. This is probably due to the ejection at the temperatures within a miscibility gap. Higher ejection temperatures resulted in formation of uniform structure of the ribbon in the scale of a light microscope, which corresponds to the region of uniform liquid above miscibility gap.
4. Higher ejection temperatures of the melt spinning process (i.e. 1403 K and more) resulted in the formation of very fine spherical particles uniformly distributed in an amorphous matrix. The spherical precipitates were crystalline and they were mainly Cu-base solid solution and M_3P type phosphide. During DTA measurement at 20 K/min, the matrix of the alloy initially amorphous, starts to crystallize at T_x = 744 K with crystallization peak at T_p = 756 K. The alloy melts between T_m = 1156 K and T_x = 1195 K, and at higher temperatures probably the two melts exist in the liquid state Fe-rich and Cu-rich. At the temperatures between $T_{d-onset}$ = 1358 K and $T_{d\text{-end-set}}$ = 1373 K the two melts transform into one homogeneous liquid.
5. Alloying the simple ternary Fe–Cu–P system with miscibility gap with Ni, Si and B provides substantially lower range of melting temperatures and it also decreases the miscibility gap.

Acknowledgment

This work is supported by the grant no. N508 024 32/1876 of Polish Ministry of Science and Higher Education.

References

[1] H. Warlimont, Mater. Sci. Eng. A304–306 (2001) 61–67.
[2] A. Makino, T. Hatanai, A. Inoue, T. Masumoto, Mater. Sci. Eng. A 226–228 (1997) 594–602.
[3] T. Kulik, J. Non-Cryst. Solids 287 (2001) 145–161.
[4] S.-W. Lee, M.-Y. Huh, E. Fleury, J.-C. Lee, Acta Mater. 54 (2006) 349–355.
[5] F. Szuecs, C.P. Kim, W.L. Johnson, Acta Mater. 49 (2001) 1507–1513.
[6] H. Choi-Yim, R.D. Conner, W.L. Johnson, Ann. Chim. Sci. Mat. 27/5 (2002) 113–118.
[7] H. Tan, Y. Zhang, Y. Li, Intermetallics 10–11 (2002) 1203–1205.
[8] Q. Wang, J.-J. Balandin, M. Suery, B. Van de Moortele, J.-M. Pelletier, All. Chim. Sci. Mat. 27/5 (2002) 19–24.
[9] X. Hu, S.C. Ng, Y.P. Feng, Y. Li, Acta Mater. 51 (2003) 561–572.
[10] U. Kühn, J. Eckert, N. Mattern, L. Schultz, Appl. Phys. Lett. 80/14 (2002) 2478–2480.
[11] C. Fan, R.T. Ott, T.C. Hufnagel, Appl. Phys. Lett. 81/6 (2002) 1020–1022.
[12] N. Mattern, Structure formation of metallic glasses, Kolloquium "Microstructure Analysis in the Materials Science", 56. Berg – und Huettenmaennischer Tag, Freiberg, 15–17.6.05 (2005).
[13] N. Mattern, U. Kuehn, A. Gebert, T. Gemming, M. Zinkevich, H. Wendrock, et al., Scripta Mater. 53/3 (2005) 271–274.
[14] B.J. Park, H.J. Chang, D.H. Kim, W.T. Kim, Appl. Phys. Lett. (2004) 6353–6355.
[15] http://www-db1.imr.tohoku.ac.jp/java_applet/Amor_Ternary/amorphous_ternary.html.
[16] P. Villars, A. Prince, H. Okamoto (Eds.), Handbook of Ternary Phase Diagrams, ASM International, 1995.
[17] F.R. Boer, R. Boom, W.C.M. Mattens, A.R. Miedema, A.K. Niessen, Cohesion and structure. Cohesion in metals, vol. 1, Elsevier Science, Amsterdam, 1988.
[18] V.T. Witusiewicz, J. Alloys Compd. 221 (1995) 74–85.
[19] A.A. Kundig, M. Ohnuma, D.H. Ping, T. Ohkubo, K. Hono, Acta Mater. 52 (2004) 2441–2448.
[20] T. Kozieł, Z. Kędzierski, A. Zielińska-Lipiec, J. Latuch, J. Microsc., in press.
[21] J.H. Perepezko, G. Wilde, J. Non-Cryst. Solids 274 (2000) 241–281.
[22] M.H. Braga, J. Vizdal, A. Kroupa, J. Ferriera, D. Soares, L.F. Malheiros, Calphad 31 (2007) 468–478.